



**HAL**  
open science

# Precipitating Fraction, Not Intensity, Explains Extreme Coarse-Grained Precipitation Clausius-Clapeyron Scaling With Sea Surface Temperature Over Tropical Oceans

Rémy Roca, Victorien de Meyer, Caroline Muller

► **To cite this version:**

Rémy Roca, Victorien de Meyer, Caroline Muller. Precipitating Fraction, Not Intensity, Explains Extreme Coarse-Grained Precipitation Clausius-Clapeyron Scaling With Sea Surface Temperature Over Tropical Oceans. *Geophysical Research Letters*, 2022, 49, 10.1029/2022GL100624 . insu-03993972

**HAL Id: insu-03993972**

**<https://insu.hal.science/insu-03993972>**

Submitted on 19 Feb 2023

**HAL** is a multi-disciplinary open access archive for the deposit and dissemination of scientific research documents, whether they are published or not. The documents may come from teaching and research institutions in France or abroad, or from public or private research centers.

L'archive ouverte pluridisciplinaire **HAL**, est destinée au dépôt et à la diffusion de documents scientifiques de niveau recherche, publiés ou non, émanant des établissements d'enseignement et de recherche français ou étrangers, des laboratoires publics ou privés.



Distributed under a Creative Commons Attribution - NonCommercial - ShareAlike 4.0 International License

# Geophysical Research Letters<sup>®</sup>

## RESEARCH LETTER

10.1029/2022GL100624

### Key Points:

- A theoretical scaling for coarse-grained extreme precipitation is introduced
- Observations reveal that the fraction of fine-scale precipitation within  $1^\circ \times 1^\circ$  domains explains the Clausius-Clapeyron scaling of coarse-grained extreme precipitation with SST
- The results are robust to the choice of satellite products used for precipitation

### Supporting Information:

Supporting Information may be found in the online version of this article.

### Correspondence to:

R. Roca,  
[remy.roca@legos.obs-mip.fr](mailto:remy.roca@legos.obs-mip.fr)

### Citation:

Roca, R., De Meyer, V., & Muller, C. (2022). Precipitating fraction, not intensity, explains extreme coarse-grained precipitation Clausius-Clapeyron scaling with sea surface temperature over tropical oceans. *Geophysical Research Letters*, 49, e2022GL100624. <https://doi.org/10.1029/2022GL100624>

Received 23 AUG 2022

Accepted 13 DEC 2022

## Precipitating Fraction, Not Intensity, Explains Extreme Coarse-Grained Precipitation Clausius-Clapeyron Scaling With Sea Surface Temperature Over Tropical Oceans

Rémy Roca<sup>1</sup> , Victorien De Meyer<sup>1</sup> , and Caroline Muller<sup>2,3</sup> 

<sup>1</sup>Laboratoire d'Etudes en Géophysique et Océanographie Spatiales, Université de Toulouse III, CNRS, CNES, IRD, Toulouse, France, <sup>2</sup>Laboratoire de Météorologie Dynamique/IPSL, ENS, PSL Université, École Polytechnique, Institut Polytechnique de Paris, Sorbonne Université, CNRS, Paris, France, <sup>3</sup>Institute of Science and Technology Austria ISTA, Klosterneuburg, Austria

**Abstract** The sensitivity of coarse-grained daily extreme precipitation to sea surface temperature is analyzed using satellite precipitation estimates over the 300–302.5 K range. A theoretical scaling is proposed, linking changes in coarse-grained precipitation to changes in fine-scale hourly precipitation area fraction and changes in conditional fine-scale precipitation rates. The analysis reveals that the extreme coarse-grained precipitation scaling with temperature ( $\sim 7\%/K$ ) is dominated by the fine-scale precipitating fraction scaling ( $\sim 6.5\%/K$ ) when using a 3 mm/h fine-scale threshold to delineate the precipitating fraction. These results are shown to be robust to the selection of the precipitation product and to the percentile used to characterize the extreme. This new coarse-grained scaling is further related to the well-known scaling for fine-scale precipitation extremes, and suggests a compensation between thermodynamic and dynamic contributions or that both contributions are small with respect to that of fractional coverage. These results suggest that processes responsible for the changes in fractional coverage are to be accounted for to assess the sensitivity of coarse-grained extreme daily precipitation to surface temperature.

**Plain Language Summary** This study focuses on the processes in the atmosphere that govern extreme coarse-grained daily precipitation over the 300–302.5 K range. It relies on theoretical developments and satellite observations, to show the importance of the fractional area coverage of fine-scale hourly precipitation to the scaling of extreme coarse-grained daily precipitation in the tropics. Our work completes and extends the existing body of theoretical knowledge on the topic, and clarifies the fundamental differences between small-scale instantaneous and coarse-grained extremes of precipitation. Our findings open new venues for understanding climate change simulations from cloud-resolving and earth system models by pointing toward the underappreciated fractional precipitation coverage as a key element of coarsened-grained extreme precipitation physics.

## 1. Introduction

At global scale, energy and water conservation laws provide a physically sound perspective on the water cycle evolution in a warmer climate (Allan et al., 2020; O’Gorman et al., 2012; Stephens et al., 2020). On the other hand, quantifying future changes of the tail of the precipitation distribution is more challenging, due to the lack of such global constraints (Pendergrass, 2020; Tapiador et al., 2019; Venugopal et al., 2018). Indeed, extreme local precipitation rates do not need to satisfy global constraints.

Nevertheless, over the last decade, the understanding of the sensitivity of intensity of short term (<1 h), small scale (<10 km) extreme events to warming has made significant progress (Fowler et al., 2021; O’Gorman, 2015). The convective dynamics and the thermodynamics of the extreme precipitation intensity sensitivity to warming have been explored using extreme-relevant simplifications of a single convective plume model. A robust feature is that the thermodynamic contribution to the sensitivity of extreme precipitation intensity to surface conditions dominates the extreme precipitation response with less important but competing effects of the convective dynamical contribution and a weak contribution of the microphysical effects (Muller & Takayabu, 2020). The thermodynamic contribution has further been related to surface humidity at saturation and shown to scale with surface temperature at the Clausius-Clapeyron (CC) rate (O’Gorman & Schneider, 2009). These theoretical developments have been assessed using various observations and models (Fischer & Knutti, 2016).

© 2022. The Authors.

This is an open access article under the terms of the [Creative Commons Attribution-NonCommercial-NoDerivs License](https://creativecommons.org/licenses/by-nc-nd/4.0/), which permits use and distribution in any medium, provided the original work is properly cited, the use is non-commercial and no modifications or adaptations are made.

At much coarser scales (>24 hr, >100 km), multiday events are not straightforwardly linked to deep convection and can involve a sequence of shorter-term precipitating events connected through synoptic wave activity. The single plume model cannot be easily invoked anymore. Extreme accumulations of multiday events are associated with a cut-off scale that increases with warming yielding a *biggest-get-bigger* effect and does not exhibit a simple scaling with surface temperature (Neelin et al., 2017).

Similarly, at the intermediate daily  $1^\circ \times 1^\circ$  scale, extreme precipitation is associated with long-lived organized mesoscale convective systems (Roca & Fiolleau, 2020). Theoretical developments are hampered by the lack of substitute for the single plume model. Idealized cloud-resolving model simulations exhibit very different behaviors (Bao, Sherwood, Colin, & Dixit, 2017; C. Muller, 2013; Singleton & Toumi, 2013) with scaling ranging from zero to 7%/K up to 14%/K (2x CC rate). This spread is notably due to the use of different models, to different warming assumptions (following a moist adiabat or constant with height), or owing to different cloud mesoscale organization (Bao, Sherwood, Alexander, & Evans, 2017; Fildier et al., 2021), and prevents unequivocal identification of key processes so far. Recent observations of  $1^\circ \times 1^\circ$  daily precipitation over tropical oceans show a robust scaling of 6%/K  $\pm$  1%/K based on multiple satellite precipitation and SST products, despite large variability in the precipitation extremes magnitude among the products (De Meyer & Roca, 2021; hereafter DMR21). DMR21 also show that the SST range (300–302.5 K) that yields a CC-like increase of the 99.9th percentile of coarse-grained precipitation, is robust to the selection of the SST and precipitation products. On the model side, such coarse-grained extremes respond to surface warming, as detailed in aquaplanet simulations, with CC-like rate (O’Gorman et al., 2021). Yet for these coarse-grained precipitation extremes at  $1^\circ \times 1^\circ \times 1$  day, the link between vertical velocity, moist static stability and extreme precipitation changes is not conclusive, confirming our limited understanding of the processes at play.

Here we explore coarse-grained extreme precipitation events, by attempting to decipher the sensitivity of the frequency versus intensity of the individual fine-scale deep convective cells to surface warming using high resolution (<10 km; hourly) satellite precipitation estimates, and a new theoretical scaling. We show that the CC-like scaling of extreme coarse-grained precipitation with SST is due to the fine-scale precipitating fraction, and not intensity, change with SST.

## 2. Data and Method

### 2.1. Satellite Precipitation Data Sets

The distribution of instantaneous fine-scale rain rates which aggregate to coarse-grained precipitation extreme events is investigated using only satellite-based precipitation estimates that resolve sub-diurnal scale at a fine spatial resolution. We further focus on so-called merged products that include both infrared and passive microwave information from the Global Precipitation Constellation owing to their overall better performances compared to single source products (Roca et al., 2021).

Three major products meet these requirements. The Global Satellite Mapping of Precipitation (GSMaP) product provides precipitation estimations using satellite observations from multiple microwave imagers and sounders as well as space borne radars at  $0.1^\circ \times 0.1^\circ$  and hourly resolution (Kubota et al., 2020). Version 6 of the NRT product is used. The Integrated Multi-satellite Retrievals for the Global Precipitation Measurement (GPM) Mission (IMERG) IMERG (Huffman et al., 2020) product consists in precipitation rates estimates on a regular  $0.1^\circ \times 0.1^\circ$  grid every 30 min. It is based on various inter-calibrated sources of precipitation data: microwave imagers and sounders observations as well as infrared brightness temperature. The version 6 of the Final Calibrated product is used. The Climate Prediction Center (CPC) morphing technique (CMORPH) Version 1.0 precipitation product is described in Xie et al. (2017). Precipitation estimates are provided on a regular grid ( $\sim$ 8 km) every 30 min. More information on these products is available in Roca et al. (2019).

### 2.2. Sea Surface Temperature

The Operational Sea Surface Temperature and Ice Analysis (OSTIA) product (Donlon et al., 2012) is used. This product relies on IR measurements from the Advanced Very High-Resolution Radiometer (AVHRR) instruments onboard the NOAA satellites as well as the multi-channel Along Track Scanning Radiometer (ATSR) and the ENVISAT Advanced Along-Track Scanning Radiometer (AATSR). Microwave based SST estimates from

Advanced Microwave Scanning Radiometer for Earth (AMSR-E) and the Tropical Rainfall Measuring Mission (TRMM) Microwave Imager (TMI) data products are also used. All of these data are blended together with in-situ measurements thanks to a multi-scale optimal interpolation technique using a 3-day assimilation window and ~100 km error correlation scale in the tropics. As discussed in DMR21, the IR cloud screening effect and the interpolation parameters both concur to building a “synoptic” foundational SST record.

### 2.3. Implementation Aspects

As discussed in the Introduction, coarse-grained is here associated with the  $1^\circ \times 1^\circ$  daily scale. The daily  $1^\circ \times 1^\circ$  statistics of precipitation are obtained from the fine-scale precipitation ( $0.1^\circ$ ; hourly instantaneous) by accumulating in space and averaging in time. The coarse-grained precipitation is further decomposed into a precipitating fraction (fraction of time and spatial fine-scale precipitation above a given threshold) and a conditional precipitation rate (average of fine-scale precipitation above a given threshold), for various thresholds applied to the satellite precipitation estimates at full space and time resolution ( $0.1^\circ$ ; hourly instantaneous). The entire 2012–2016 period for the whole tropical belt ( $30^\circ\text{S}$ – $30^\circ\text{N}$ ) ocean is processed as previously deemed adequate for scaling analysis (DMR21).

The *local* surface temperature is used to compute a scaling for the tropics following previous efforts (Roca, 2019; DMR21). In order to avoid the cooling effect of the contemporaneous extreme precipitation event at the surface, which alters the estimated scaling between precipitation and temperature, a time-lag relationship between the extreme precipitation and the surface temperature is used (e.g., Bao, Sherwood, Alexander, & Evans, 2017). For tropical oceans, DMR21 have shown that a 2 days lag performs well to alleviate the cooling effect when considering three different SST products. All daily  $1^\circ \times 1^\circ$  grid boxes are then pooled together into 0.5 K *local, lagged* SST bins to form the precipitation amount distribution. Wet-days ( $P > 1$  mm/d) percentiles are then calculated and high percentiles of the distribution, from 99th up to 99.99th, are used as markers of extreme coarse-grained precipitation. Wet days percentiles are preferred over all-days percentiles since it is better suited for scaling analysis as argued in Schär et al. (2016). The value of precipitation at a given percentile is then calculated as the averaged precipitation falling within 5% of the percentile's precipitation value. As noted in the Introduction, DMR21 show that the SST range that robustly yields a CC-like increase of extreme coarse-grained precipitation is 300–302.5 K. They further show that the CC-scaling shows negligible sensitivity to the temperature-precipitation time lag between 1 and 2 days. Based on these observational results, we focus here on the scaling of extreme coarse-grained precipitation with SST, as measured by the ratio between the 302–302.5 K and the 300–300.5 K precipitation percentile bins, over this 2 K SST range.

## 3. A New Scaling for Coarse Grained Extreme Precipitation Amount With Surface Temperature

### 3.1. Formulation

With the  $[\cdot]$  denoting time averaging and the overbar spatial averaging, the coarse-grained precipitation amount  $[\overline{P}]$  in mm can be decomposed as follows

$$[\overline{P}] = \alpha_p \times [\overline{P}_p] \quad (1)$$

where  $[\overline{P}_p]$  in mm is the space/time amount of fine-scale precipitation  $P$  ( $0.1^\circ$ ; hourly instantaneous) above a threshold  $p$  (subscript). Writing  $\alpha_p = [\overline{P}] / [\overline{P}_p]$ , the unitless coefficient  $\alpha_p$  can be thought of the inverse of the contribution of  $[\overline{P}_p]$  (only accounting for fine-scale precipitation above the threshold  $p$ ) to  $[\overline{P}]$  (including all fine-scale precipitation). The coarse-grained thresholded precipitation amount  $[\overline{P}_p]$  can further be decomposed as

$$[\overline{P}_p] = \sigma_p \times [\overline{R_{\text{cond}p}}] \times D \quad (2)$$

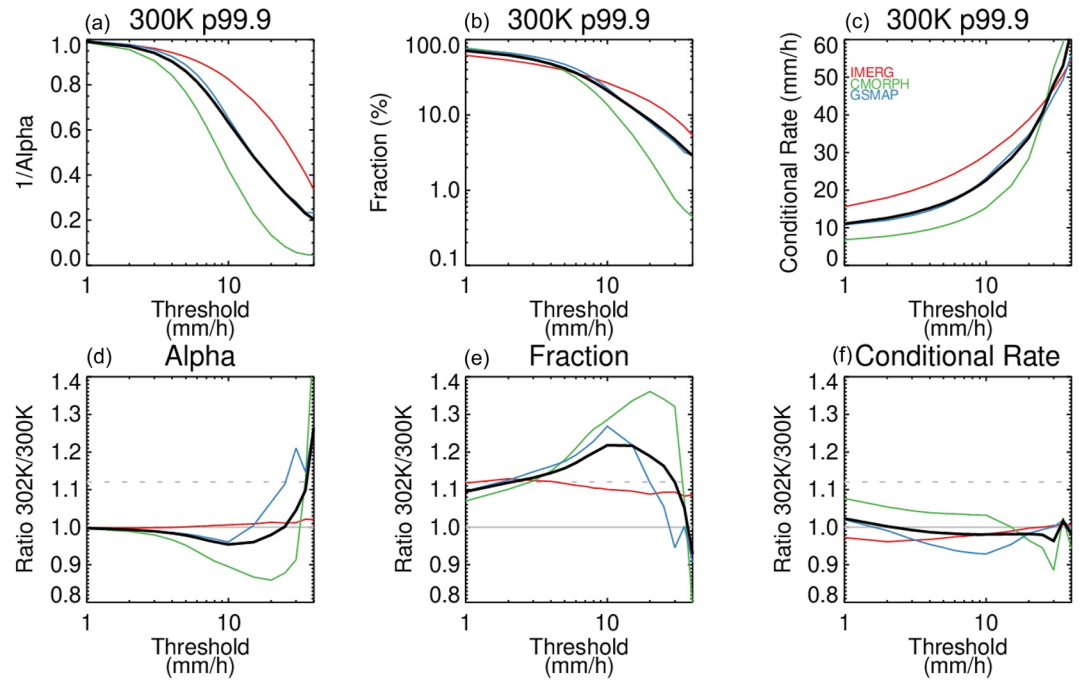


**Figure 1.** The terms of Equation 2 for the 99.9 percentile as a function of the fine scale threshold. (top) At 300 K. (bottom) ratio between 302 and 300 K. For alpha (a, d) the precipitating fraction (b, e) and the conditional rate (c, f). Colors correspond to individual products and the multiproducts mean is plotted in black. In the bottom panels, the dashed gray horizontal line is the Clausius-Clapeyron rate.

where  $\sigma_p$  is the fraction of the space/time domain for which the fine-scale precipitation rate exceeds the threshold  $p$  and  $\overline{R_{cond p}}$  (in mm/h) is the mean of the fine-scale precipitation rate when it precipitates above the threshold  $p$ .  $D$  is the duration of the time integral (here set to 24 hr).

A scaling for coarse-grained precipitation amount can then be derived writing the incremental change in  $\overline{P}$  that now reads

$$\frac{\delta \overline{P}}{\overline{P}} \sim \frac{\delta \alpha_p}{\alpha_p} + \frac{\delta \sigma_p}{\sigma_p} + \frac{\delta \overline{R_{cond p}}}{\overline{R_{cond p}}} + \text{residual} \quad (3)$$

The scaling can be approximated as the sum of three terms: the scaling of contribution of  $\overline{P_p}$  to  $\overline{P}$ , the scaling of the precipitating fraction and the scaling of the conditional mean precipitation rates and a residual corresponding to higher order terms. We note that such an expression as Equation 1 forms the basis of numerous satellite accumulated precipitation products algorithms (Guilloteau et al., 2016; Roca et al., 2018; Tapiador et al., 2012) and while we use it for extreme coarse-grained precipitation amount, it actually holds for any coarse-grained precipitation amount and no extreme-specific assumptions are introduced in its derivation. The distribution of the precipitation and of these terms are shown for reference in Figure S1 in Supporting Information S1 for two thresholds and will be discussed in the course of this Letter.

### 3.2. Sensitivity to the Selection of the Fine Scale Threshold

At 300 K and for the 99.9th percentile of the daily  $1^\circ \times 1^\circ$  precipitation, the inverse of the contribution of  $\overline{P_p}$  to the precipitation (Figure 1a) exhibits a strong decrease for thresholds above 5 mm/h ranging from  $\sim 90\%$  to less than 20% when considering the ensemble mean of the products. This steep decrease is robust among the products

**Table 1**  
Scaling Values of the Terms of Equation 2 for a Threshold of 3 mm/h and the 99.9 Percentile

Products	$\frac{\delta \bar{P}}{ \bar{P} }$	$\frac{\delta \alpha_{3\text{mm/h}}}{\alpha_{3\text{mm/h}}}$	$\frac{\delta \sigma_{3\text{mm/h}}}{\sigma_{3\text{mm/h}}}$	$\frac{\delta \left[ \frac{R_{\text{cond}3\text{mm/h}}}{R_{\text{cond}3\text{mm/h}}} \right]}{\left[ \frac{R_{\text{cond}3\text{mm/h}}}{R_{\text{cond}3\text{mm/h}}} \right]}$	Residual
IMERG	5.1	0.0	6.2	-1.7	0.6
CMORPH	8.3	-1.2	6.1	2.2	1.2
GSMAP	7.2	-0.5	7.4	-1.6	1.9
Mean	6.9	-0.6	6.6	-0.4	1.2
Std	1.7	0.6	0.7	2.2	0.7

Note. Units are %/K.

although its rate is much stronger for CMORPH than for the other two. From 1 to ~3 mm/h, the contribution is steady of the order of 95% of the original precipitation amount and this feature is also robust to the selection of the product. The precipitating fraction (Figure 1b) also decreases with the threshold but more regularly than for the contribution. The products agree among each other up to ~7 mm/h and, above that, are characterized by different intensities in line with the analysis of the contribution. Figure 1c shows the conditional rain rate as a function of the threshold. The three products agree on the shape of the dependency with a small sensitivity up to ~7 mm/h followed by a steep increase as the threshold increases. All together, this decomposition reveals that the distribution of instantaneous rates in the satellite precipitation products exhibits robust key features despite strong differences in the most intense instantaneous precipitation rate occurrence.

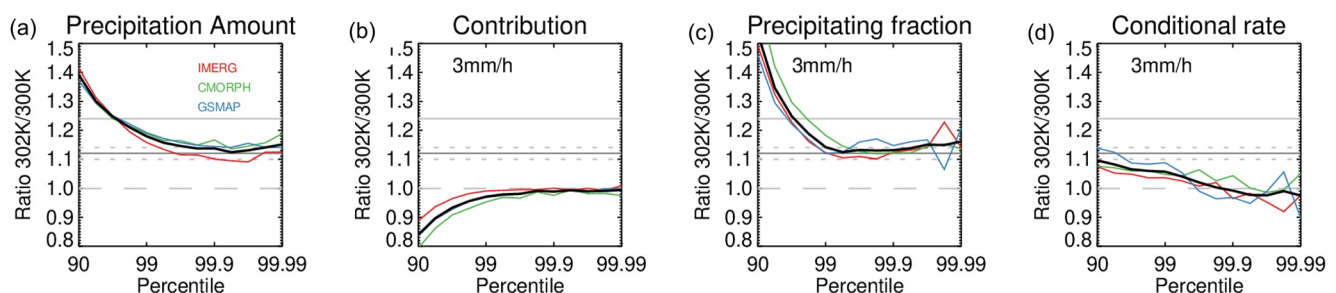
The sensitivity of the scaling to the threshold is investigated as well.

Figure 1d shows that the contribution is not sensitive to the SST up to a threshold of ~3 mm/h; a robust aspect among the products. Above this value, the scaling of the contribution becomes product-dependent and ranges from slightly negative (IMERG) to very positive (CMORPH). The scaling of the precipitating fraction is close to the Clausius-Clapeyron rate around 3 mm/h for all products while for larger thresholds, it is characterized by large and product-dependent fluctuations (Figure 1e). The conditional rate scaling does not express much sensitivity to the threshold and is on average close to one, slightly above (below) for thresholds lower (higher) than 3 mm/h. Using the scaling of Equation 3 yields to a small positive residual that becomes slightly negative above 5–6 mm/h, with ensemble mean residual ranging between -2 and 1.2%/K (Figure S2 in Supporting Information S1).

For the 99.9th percentile, selecting a threshold of 3 mm/h well represents the total precipitation over the SST range used here for the scaling computation. It further allows decomposition of the scaling using Equation 3 whose individual terms are quantified in Table 1. The ensemble mean residual is small, 1.2%/K and smaller than the standard deviation of the ensemble precipitation scaling (1.7%/K) indicating the relevance of the scaling approximation. Comparing the individual terms shows that the precipitation fraction scaling is the dominant term of the budget, a feature common to all products, with a value close to Clausius-Clapeyron scaling of  $6.6 \pm 0.7\%/K$ . The second term in magnitude is the conditional rate scaling followed by the contribution term. The former exhibits sign changes among the products while the latter is non positive for all the products. In summary, the extreme precipitation amount scaling is dominated, when using a 3 mm/h threshold, by the precipitation fraction scaling with CC like values, the departure from CC being due to compensating effects between the much smaller contributions, conditional rate and the residual.

### 3.3. Sensitivity to the Percentile

The sensitivity of the results to the selection of a given percentile of the distribution is investigated keeping the same fine scale threshold of 3 mm/h. The conclusions for the 99.9 percentile case (~170 mm/d; Figure S1a in Supporting Information S1) hold from a broad range of percentiles from 99.5 to 99.99 (Figure 2). This



**Figure 2.** The ratio between 302 and 300 K for each of the terms of Equation 2 for the fine scale threshold of 3 mm/h as a function of the percentile. For precipitation amount (a) the contribution (b) the precipitating fraction (c) and the conditional rate (d). Colors correspond to individual products and the multiproducts mean is plotted in black. In the bottom panels, the horizontal gray line is the Clausius-Clapeyron rate plus or minus 1%/K indicated by the dotted lines. The other plain gray line is 2xCC and the dashed gray line corresponds to a ratio of 1.

corresponds to daily  $1^\circ \times 1^\circ$  accumulation precipitation ranging from 105 to  $\sim 280$  mm/d for the multi products mean (Figure S1a in Supporting Information S1). This indicates that the same processes appear to control intense precipitation events ranging from “moderate” to “extreme” extreme precipitation daily amount.

#### 4. Summary and Discussion

The theoretical rationale for the scaling of coarse-grained extreme precipitation amount with sea surface temperature over the tropics is revisited. An observational constraint on the scaling is obtained by using multiple satellite precipitation products and foundational SST over warm tropical oceans. The results show that, once a 2 days lag is accounted for in the joint precipitation-temperature analysis to mitigate the cooling effect of the intense precipitation on the contemporaneous surface temperature, the coarse-grained extreme precipitation amount scaling is  $\sim 6.9\%/K$ . The theoretical framework is completed in order to deconvolve the role of the precipitating fractional coverage from the other processes linked to conditional precipitation intensity. The results show that the sensitivity of extreme time-domain-averaged precipitation amount to surface conditions is dominated by the sensitivity of the fractional coverage of fine-scale precipitation above a threshold rather than by changes in the intensity of the small scale precipitating cells. The fractional coverage scaling is further shown to be very close to the Clausius-Clapeyron rate. These results are robust to the selection of the satellite product and to the percentile selection used to define the extreme. This prompts the following two questions: how does this relate to previous scaling formulations for fine-scale single cell extreme precipitating events whose intensity increase at CC rate? And what drives the CC scaling of the precipitation fraction?

By carefully averaging the dry static energy budget equations over a spatial domain and over time (see Appendix A), the scaling of the extreme coarse-grained precipitation  $[\overline{P_e}]$  can be written as

$$[\overline{P_e}] \sim \frac{1}{L} \left[ \int \overline{\rho w \frac{\partial s}{\partial z}} \right] \quad (4)$$

where, as before, the overbar corresponds to spatial averaging and the  $[\cdot]$  to temporal averaging.  $s$  is the dry static energy  $s = c_p T + gz$  with  $c_p$  the specific heat of air at constant pressure and  $g$  the acceleration due to gravity and  $\rho$  the mass density of dry air.  $L$  is the latent heat of vaporization and  $w$  the vertical velocity. This simplified equation states that the extreme coarse-grained average precipitation can be approximated by the time averaged vertically integrated product of domain mean vertical dynamics and thermodynamics. Interestingly enough, this is very close to the budget equation of O’Gorman and Schneider (2009) and Muller et al. (2011) although we note that at this stage we have not introduced much extreme precipitation intensity related assumptions beyond the scale analysis of the r.h.s. of Equation A2. Furthermore, it is worth noting that no precipitation efficiency term appears in our derivation, unlike earlier scalings at finer convective scale (Muller et al., 2011), since, as noted in the appendix, in our case, we assume when deriving Equation 4 that, all the condensation leads to surface precipitation.

Further noting  $\sigma$  the precipitating fraction over the space-time domain, we write with the  $p(d)$  subscript corresponding to precipitating (non-precipitating) part of the domain respectively

$$\overline{w} = \sigma \overline{w_p} + (1 - \sigma) \overline{w_d} \quad (5)$$

Formulating the following assumptions for extreme coarse-grained precipitation:

1.  $\sigma$  is not small compared to 1
2.  $\sigma$  is independent of  $z$  and set to its surface value
3. and  $\overline{w_p} > \overline{w_d}$

We can rewrite

$$[\overline{P_e}] \sim \sigma \frac{1}{L} \left[ \int \overline{\rho w_p \frac{\partial s}{\partial z}} \right] \quad (6)$$

Under differentiation, the incremental change in extreme daily averaged precipitation amount over the domain  $[\overline{P_e}]$  can be now written, neglecting the higher-order terms,

$$\frac{\delta \left[ \overline{P_e} \right]}{\left[ \overline{P_e} \right]} \sim \frac{\delta \sigma}{\sigma} + \frac{\left[ \int \overline{\rho w_p} \delta \left( \frac{\partial \bar{s}}{\partial z} \right) \right]}{\left[ \int \overline{\rho w_p} \frac{\partial \bar{s}}{\partial z} \right]} + \frac{\left[ \int \delta \left( \overline{\rho w_p} \right) \frac{\partial \bar{s}}{\partial z} \right]}{\left[ \int \overline{\rho w_p} \frac{\partial \bar{s}}{\partial z} \right]} + \text{residual} \quad (7)$$

This decomposition consists in a fractional surface precipitation coverage term and a thermodynamic term, linked to the changes in the domain averaged dry static energy vertical gradient, and a dynamical term, associated with the changes in the precipitating mass flux. We have kept the classic delineation into thermodynamics and dynamics (e.g., Muller et al., 2011), although it should be kept in mind that, owing to our derivation and the introduction of the precipitation fractional coverage, these terms do not compare one-to-one with previously reported similar estimates. Figure S1 in Supporting Information S1 supports assumption #1 and indicates precipitation fraction over 3 mm/h, our reference threshold, ranging from 40% to 60% depending on the product and the percentiles under consideration. For a lower threshold (0 mm/h), the precipitation fraction exhibits values above 80% for percentiles above 99. Assumptions #2 and #3 are not backed up by the current datasets and correspond to first order take on deep convection dynamics and vertical distribution. These approximations might require further refinements in the future.

The consequences of our findings are that these newly formulated thermodynamic and dynamical terms cancel each other out, at the residual level. It means that, either, each term is very small and the associated processes do not come into play for coarse-grained precipitation extreme scaling, or the two terms do show significant magnitude compared to the fraction scaling term but of opposite sign. Further clarifying these terms, using the analytical path is strongly hampered by the impossibility, at coarse-grained resolution, to further simplify  $\bar{s}$ . Unlike for the instantaneous small scales, we see here no direct route to relate these terms to surface humidity at saturation, that is, the Clausius Clapeyron rate for the considered SST. It seems necessary to turn to model simulations to gain a better understanding of the fate of the thermodynamic and dynamical terms, and will be the subject of future work. At first glance, precipitating fraction could be related to water vapor convergence (Anthes, 1977), a good candidate for Clausius-Clapeyron like scaling rate with SST (Loriaux et al., 2017). At our coarse-grained scales, heavy tropical precipitation amount events are dominated by organized, long-lived convective systems (Roca & Fiolleau, 2020). The mesoscale convective systems physics hence offers a pathway linking extreme precipitation amount and precipitation fraction, possibly through convergence.

This process is consistent with recently reported trends for the ITCZ intense precipitation amount that shows an increase together with storm size yielding to larger precipitating area extent happening in conjunction with narrowing of the ITCZ (Wodzicki & Rapp, 2022). Exploring how this precipitating fraction scaling could also apply to SST warmer than 302.5 K; a regime for which flat or negative scaling has been identified in DMR21 and others that remains not fully understood (Sun & Wang, 2022) could be a venue for future research. Finally note that various agencies are reprocessing long series of high-resolution precipitation data with improved algorithms versions (GSMaP v8, IMERG v 6 and CMORPH 2) and the present study will be extended and revisited with these new generation products when available.

## Appendix A: Scaling of Extreme Precipitation at Coarse-Grained Scale From the Dry Static Budget

We consider a  $1^\circ \times 1^\circ$  domain, and re-derive the scaling approximation for extreme daily precipitation averaged over this domain. We start from heat budget considerations and as various integrals are performed (spatial, vertical, temporal), we detail the various underlying approximations and simplifications. The standard heat budget equation can be derived from the first law of thermodynamic and mass conservation arguments under a few assumptions usually appropriate for tropical conditions (Yanai et al., 1973). We start from the dry static energy equation and mass conservation equation (Schubert et al., 2018):

$$\frac{D}{Dt}(\rho s) = \rho Q_R + L\rho(c - e)$$

$$\frac{D}{Dt}(\rho) = 0$$

where  $D/Dt$  is the Lagrangian derivative,  $s$  is the dry static energy  $s = c_p T + gz$  with  $c_p$  the specific heat of air at constant pressure and  $g$  the acceleration due to gravity, and  $\rho$  the mass density of dry air.  $L$  is the latent heat of vaporization,  $c$  is the condensation rate and  $e$  the reevaporation rate;  $Q_R$  is the radiative heating rate. For the sake of simplicity, a constant,  $L$  is used here that equals neglecting ice effects on the heat budget although the budget equation accounting for ice can also be formulated.

We further split variables into horizontal averages denoted with overbars, and departures from these horizontal averages denoted by primes, and denote  $\overline{D/Dt} = \partial/\partial t + \overline{u}\partial/\partial x + \overline{v}\partial/\partial y + \overline{w}\partial/\partial z$  (advection by the mean wind). We also neglect time and horizontal variations in density  $\rho \approx \overline{\rho}(z)$ , as well as horizontal eddy flux terms involving horizontal gradients of  $\overline{u's'}$  or  $\overline{v's'}$ , due to the small horizontal temperature gradients in the tropics (weak temperature gradient approximation, Sobel et al., 2001). Thus, the above equations averaged become

$$\begin{aligned} \overline{\rho} \frac{\overline{D}}{\overline{Dt}} \overline{s} &= \overline{\rho} \overline{Q_R} + L \overline{\rho} (\overline{c} - \overline{e}) - \frac{\partial (\overline{\rho w' s'})}{\partial z} \\ \frac{\partial}{\partial x} (\overline{\rho u}) + \frac{\partial}{\partial y} (\overline{\rho v}) + \frac{\partial}{\partial z} (\overline{\rho w}) &= 0 \end{aligned} \quad (A1)$$

Upon vertical integration, Equation 1 becomes

$$\int \overline{\rho} \frac{\overline{D}}{\overline{Dt}} \overline{s} = \int \overline{\rho} \overline{Q_R} + L \overline{P} - \overline{F_{sh}} \quad (A2)$$

where the integral sign indicates integral  $\int_{z=0}^{z=op} (\cdot) dz$  from surface to the top of the atmosphere,  $\overline{F_{sh}}$  the sensible heat flux at the surface,  $\overline{P}$  the precipitation rate at the surface.  $\overline{Q_R}$  is the radiative heating. All the rhs terms should be understood as domain-averages. In obtaining Equation 2, the latent heating due to clouds that do not precipitate has been neglected. It is difficult to assess if the latter approximation holds at the daily  $1^\circ \times 1^\circ$  scale of interest here (Johnson et al., 2015) although for its omission to be significant, it would require unlikely significant lateral cloud material export (Kato et al., 2016). Note though that at smaller, cloud-like kilometric scale, cloud condensate accumulation and lateral advection would make this approximation questionable, and the introduction of a precipitation efficiency would be necessary to be consistent with earlier small-scale scalings (e.g., Muller et al., 2011).

In the tropics, following the weak temperature gradient approximation (Sobel et al., 2001), the dry static budget is often further simplified,

$$\overline{\rho} \frac{\overline{D}}{\overline{Dt}} \overline{s} \sim \overline{\rho w} \frac{\partial \overline{s}}{\partial z}$$

Such an assumption seems to hold for tropical conditions and at the scales of interest here (Betts, 1997; Sobel et al., 2014).

If we now also consider temporally averaged quantities, scale analysis permits further simplification of the r.h.s. of Equation A2 under heavy daily precipitation conditions. Considering a typical  $1^\circ \times 1^\circ$  daily intense event with a precipitation amount of 100 mm/d, it corresponds roughly to  $\sim 3,000 \text{ Wm}^{-2}$  heating of the atmospheric column during that day. Climatologically, over tropical oceans, the sensible heat flux is much smaller than the precipitation term (e.g., Kato et al., 2016) and recent observations over the Indian Ocean further confirm this scale analysis with  $F_{sh} \sim 10 \text{ Wm}^{-2}$  for typical intense precipitation event at the  $1^\circ \times 1^\circ$  daily scale (Johnson et al., 2015). The radiative cooling term is also often neglected due to its smaller magnitude compared to the precipitation term (L'Ecuyer & Stephens, 2003). Over the western part of the tropical Pacific Ocean, during the TOGA-COARE campaign, daily vertically averaged  $\overline{Q_R}$  oscillates around  $\pm 1 \text{ K/day}$ , roughly  $\pm 100 \text{ Wm}^{-2}$  (Johnson and Cieliecki, 2000) still very small compared to precipitation warming. Expressing time averaging with the  $[\cdot]$  operator and the above-mentioned simplifications, the average extreme precipitation can be approximated by

$$[\overline{P_e}] \sim \frac{1}{L} \left[ \int \overline{\rho w} \frac{\partial \overline{s}}{\partial z} \right]$$

## Data Availability Statement

IMERG Final Calibrated is identified with the <https://doi.org/10.5067/GPM/IMERG/3B-HH/06> IMERG Early Uncal is identified with the <https://doi.org/10.5067/GPM/IMERG/3B-HH-E/06>. CMORPH is identified with the <https://doi.org/10.25921/w9va-q159>. GSMaP data are available at <https://sharaku.eorc.jaxa.jp/GSMaP/>. OSTIA SST are identified with the <https://doi.org/10.48670/moi-00165>.

## Acknowledgments

We thank S. Cloché for her support with the handling of these various data sets. This study benefited from the IPSL meso-center ESPRI facility which is supported by CNRS, UPMC, Labex L-IPSL, CNES and Ecole Polytechnique. We thank Rômulo A. Jucá Oliveira and Thomas Fiolleau for helpful discussions on satellite data and precipitation. The authors acknowledge the CNES and CNRS support under the Megha-Tropiques program. C.M. gratefully acknowledges funding from the European Research Council (ERC) under the European Union's Horizon 2020 research and innovation programme (Project CLUSTER, Grant agreement 805041). We further thank the reviewers for their insightful comments that improved the paper.

## References

- Allan, R. P., Barlow, M., Byrne, M. P., Cherchi, A., Douville, H., Fowler, H. J., et al. (2020). Advances in understanding large-scale responses of the water cycle to climate change. *Annals of the New York Academy of Sciences*, 1472(1), 49–75. <https://doi.org/10.1111/nyas.14337>
- Anthes, R. A. (1977). A cumulus parameterization scheme utilizing a one-dimensional cloud model. *Monthly Weather Review*, 105(3), 270–286. [https://doi.org/10.1175/1520-0493\(1977\)105<0270:acpsua>2.0.co;2](https://doi.org/10.1175/1520-0493(1977)105<0270:acpsua>2.0.co;2)
- Bao, J., Sherwood, S. C., Alexander, L. V., & Evans, J. P. (2017). Future increases in extreme precipitation exceed observed scaling rates. *Nature Climate Change*, 7(2), 128–132. <https://doi.org/10.1038/nclimate3201>
- Bao, J., Sherwood, S. C., Colin, M., & Dixit, V. (2017). The robust relationship between extreme precipitation and convective organization in idealized numerical modeling simulations. *Journal of Advances in Modeling Earth Systems*, 9(6), 2291–2303. <https://doi.org/10.1002/2017MS001125>
- Betts, A. K. (1997). The parameterization of deep convection. In R. K. Smith (Ed.), *The physics and parameterization of deep convection* (pp. 255–279). Kluwer Academic Publishers.
- De Meyer, V., & Roca, R. (2021). Thermodynamic scaling of extreme daily precipitation over the tropical ocean from satellite observations. *Journal of the Meteorological Society of Japan*, 99(2), 423–436. <https://doi.org/10.2151/jmsj.2021-020>
- Donlon, C. J., Martin, M., Stark, J., Roberts-Jones, J., Fiedler, E., & Wimmer, W. (2012). The operational sea surface temperature and sea ice analysis (OSTIA) system. *Remote Sensing of Environment*, 116, 140–158. <https://doi.org/10.1016/j.rse.2010.10.017>
- Fildier, B., Collins, W. D., & Muller, C. (2021). Distortions of the rain distribution with warming, with and without self-aggregation. *Journal of Advances in Modeling Earth Systems*, 13(2), e2020MS002256. <https://doi.org/10.1029/2020MS002256>
- Fischer, E. M., & Knutti, R. (2016). Observed heavy precipitation increase confirms theory and early models. *Nature Climate Change*, 6(11), 986–991. <https://doi.org/10.1038/nclimate3110>
- Fowler, H. J., Ali, H., Allan, R. P., Ban, N., Barbero, R., Berg, P., et al. (2021). Towards advancing scientific knowledge of climate change impacts on short-duration rainfall extremes. *Philosophical Transactions of the Royal Society A: Mathematical, Physical and Engineering Sciences*, 379(2195). <https://doi.org/10.1098/rsta.2019.0542>
- Guilloteau, C., Roca, R., & Gosset, M. (2016). A multiscale evaluation of the detection capabilities of high-resolution satellite precipitation products in West Africa. *Journal of Hydrometeorology*, 17(7), 2041–2059. <https://doi.org/10.1175/JHM-D-15-0148.1>
- Huffman, G. J., Bolvin, D. T., Braithwaite, D., Hsu, K. L., Joyce, R. J., Kidd, C., et al. (2020). Integrated multi-satellite retrievals for the global precipitation measurement (GPM) mission (IMERG). 343–353. [https://doi.org/10.1007/978-3-030-24568-9\\_19](https://doi.org/10.1007/978-3-030-24568-9_19)
- Johnson, R. H., & Ciesielski, P. E. (2000). Rainfall and radiative heating rates from TOGA COARE atmospheric budgets. *Journal of the Atmospheric Sciences*, 57(10), 1497–1514. [https://doi.org/10.1175/1520-0469\(2000\)057<1497:RARHRF>2.0.CO;2](https://doi.org/10.1175/1520-0469(2000)057<1497:RARHRF>2.0.CO;2)
- Johnson, R. H., Ciesielski, P. E., Ruppert, J. H., & Katsumata, M. (2015). Sounding-based thermodynamic budgets for DYNAMO. *Journal of the Atmospheric Sciences*, 72(2), 598–622. <https://doi.org/10.1175/JAS-D-14-0202.1>
- Kato, S., Xu, K. M., Wong, T., Loeb, N. G., Rose, F. G., Trenberth, K. E., & Thorsen, T. J. (2016). Investigation of the residual in column-integrated atmospheric energy balance using cloud objects. *Journal of Climate*, 29(20), 7435–7452. <https://doi.org/10.1175/JCLI-D-15-0782.1>
- Kubota, T., Aonashi, K., Ushio, T., Shige, S., Takayabu, Y. N., Kachi, M., et al. (2020). Global satellite mapping of precipitation (GSMaP) products. In V. Levizzani, C. Kidd, D. Kirschbaum, C. Kummerow, K. Nakamura, & F. J. Turk (Eds.), *The GPM Era. Satellite precipitation measurement* (pp. 355–373). Springer.
- L'Ecuyer, T. S., & Stephens, G. L. (2003). The tropical oceanic energy budget from the TRMM perspective. Part I: Algorithm and uncertainties. *Journal of Climate*, 16(12), 1967–1985. [https://doi.org/10.1175/1520-0442\(2003\)016<1967:TTOEBF>2.0.CO;2](https://doi.org/10.1175/1520-0442(2003)016<1967:TTOEBF>2.0.CO;2)
- Loriaux, J. M., Lenderink, G., & Pier Siebesma, A. (2017). Large-scale controls on extreme precipitation. *Journal of Climate*, 30(3), 955–968. <https://doi.org/10.1175/JCLI-D-16-0381.1>
- Muller, C. (2013). Impact of convective organization on the response of tropical precipitation extremes to warming. *Journal of Climate*, 26(14), 5028–5043. <https://doi.org/10.1175/JCLI-D-12-00655.1>
- Muller, C. J., O'Gorman, P. A., & Back, L. E. (2011). Intensification of precipitation extremes with warming in a cloud-resolving model. *Journal of Climate*, 24(11), 2784–2800. <https://doi.org/10.1175/2011JCLI3876.1>
- Muller, C. J., & Takayabu, Y. (2020). Response of precipitation extremes to warming: What have we learned from theory and idealized cloud-resolving simulations, and what remains to be learned? *Environmental Research Letters*, 15(3), 035001. <https://doi.org/10.1088/1748-9326/ab7130>
- Neelin, J. D., Sahany, S., Stechmann, S. N., & Bernstein, D. N. (2017). Global warming precipitation accumulation increases above the current-climate cutoff scale. *Proceedings of the National Academy of Sciences of the United States of America*, 114(6), 1258–1263. <https://doi.org/10.1073/pnas.1615333114>
- O'Gorman, P. A. (2015). Precipitation extremes under climate change. *Current Climate Change Reports*, 1(2), 49–59. <https://doi.org/10.1007/s40641-015-0009-3>
- O'Gorman, P. A., Allan, R. P., Byrne, M. P., & Previdi, M. (2012). Energetic constraints on precipitation under climate change. *Surveys in Geophysics*, 33(3–4), 585–608. <https://doi.org/10.1007/s10712-011-9159-6>
- O'Gorman, P. A., Li, Z., Boos, W. R., & Yuval, J. (2021). Response of extreme precipitation to uniform surface warming in quasi-global aquaplanet simulations at high resolution. *Philosophical Transactions of the Royal Society A: Mathematical, Physical and Engineering Sciences*, 379(2195). <https://doi.org/10.1098/rsta.2019.0543>
- O'Gorman, P. A., & Schneider, T. (2009). The physical basis for increases in precipitation extremes in simulations of 21st-century climate change. *Proceedings of the National Academy of Sciences of the United States of America*, 106(35), 14773–14777. <https://doi.org/10.1073/pnas.0907610106>
- Pendergrass, A. G. (2020). Changing degree of convective organization as a mechanism for dynamic changes in extreme precipitation. *Current Climate Change Reports*, 6(2), 47–54. <https://doi.org/10.1007/s40641-020-00157-9>

- Roca, R. (2019). Estimation of extreme daily precipitation thermodynamic scaling using gridded satellite precipitation products over tropical land. *Environmental Research Letters*, *14*(9), 095009. <https://doi.org/10.1088/1748-9326/ab35c6>
- Roca, R., Alexander, L. V., Potter, G., Bador, M., Jucá, R., Contractor, S., et al. (2019). FROGS: A daily  $1^\circ \times 1^\circ$  gridded precipitation database of rain gauge, satellite and reanalysis products. *Earth System Science Data*, *11*(3), 1017–1035. <https://doi.org/10.5194/essd-11-1017-2019>
- Roca, R., Haddad, Z. S., Akimoto, F. F., Alexander, L., Behrangi, A., Huffman, G., et al. (2021). The joint IPWG/GEWEX precipitation assessment. In R. Roca & Z. S. Haddad (Eds.), *World climate research programme* (p. 125). WCRP.
- Roca, R., & Fiolleau, T. (2020). Extreme precipitation in the tropics is closely associated with long-lived convective systems. *Commun. Earth Environ.*, *1*, 1–6. <https://doi.org/10.1038/s43247-020-00015-4>
- Roca, R., Taburet, N., Lorant, E., Chambon, P., Alcoba, M., Brogniez, H., et al. (2018). Quantifying the contribution of the Megha-Tropiques mission to the estimation of daily accumulated rainfall in the Tropics. *Quarterly Journal of the Royal Meteorological Society*, *144*(S1), 49–63. <https://doi.org/10.1002/qj.3327>
- Schär, C., Ban, N., Fischer, E. M., Rajczak, J., Schmidli, J., Frei, C., et al. (2016). Percentile indices for assessing changes in heavy precipitation events. *Climate Change*, *137*(1–2), 201–216. <https://doi.org/10.1007/s10584-016-1669-2>
- Schubert, W. H., Ciesielski, P. E., & Johnson, R. H. (2018). Heat and moisture budget analysis with an improved form of moist thermodynamics (pp. 1–14). Retrieved from <http://arxiv.org/abs/1810.11119>
- Singleton, A., & Toumi, R. (2013). Super-Clausius-Clapeyron scaling of rainfall in a model squall line. *Quarterly Journal of the Royal Meteorological Society*, *139*(671), 334–339. <https://doi.org/10.1002/qj.1919>
- Sobel, A., Wang, S., & Kim, D. (2014). Moist static energy budget of the MJO during DYNAMO. *Journal of the Atmospheric Sciences*, *71*(11), 4276–4291. <https://doi.org/10.1175/JAS-D-14-0052.1>
- Sobel, A. H., Nilsson, J., & Polvani, L. M. (2001). The weak temperature gradient approximation and balanced tropical moisture waves. *Journal of the Atmospheric Sciences*, *58*(23), 3650–3665. [https://doi.org/10.1175/1520-0469\(2001\)058<3650:TWGTAA>2.0.CO;2](https://doi.org/10.1175/1520-0469(2001)058<3650:TWGTAA>2.0.CO;2)
- Stephens, G. L., Slingo, J. M., Rignot, E., Reager, J. T., Hakuba, M. Z., Durack, P. J., et al. (2020). Earth's water reservoirs in a changing climate. *Proceedings of The Royal Society A Mathematical Physical and Engineering Sciences*, *476*(2236), 20190458. <https://doi.org/10.1098/rspa.2019.0458>
- Sun, X., & Wang, G. (2022). Causes for the negative scaling of extreme precipitation at high temperatures. *Journal of Climate*, *35*(18), 6119–6134. <https://doi.org/10.1175/jcli-d-22-0142.1>
- Tapiador, F. J., Roca, R., Del Genio, A., Dewitt, B., Petersen, W., & Zhang, F. (2019). Is precipitation a good metric for model performance? *Bulletin American Meteorology Social*, *100*(2), 223–233. <https://doi.org/10.1175/BAMS-D-17-0218.1>
- Tapiador, F. J., Turk, F., Petersen, W., Hou, A. Y., Garcia-Ortega, E., Machado, L. A., et al. (2012). Global precipitation measurement: Methods, datasets and applications. *Atmospheric Research*, *104–105*, 70–97. <https://doi.org/10.1016/j.atmosres.2011.10.021>
- Venugopal, V., Murtugudde, R., Sukhatme, J., & Roca, R. (2018). Tropical extremes: Natural variability and trends. <https://doi.org/10.1016/C2015-0-05558-7>
- Wodzicki, K. R., & Rapp, A. D. (2022). More Intense, organized deep convection with shrinking tropical ascent regions. *Geophysical Research Letters*, *49*(15), e2022GL098615. <https://doi.org/10.1029/2022GL098615>
- Xie, P., Joyce, R., Wu, S., Yoo, S. H., Yarosh, Y., Sun, F., & Lin, R. (2017). Reprocessed, bias-corrected CMORPH global high-resolution precipitation estimates from 1998. *Journal of Hydrometeorology*, *18*(6), 1617–1641. <https://doi.org/10.1175/JHM-D-16-0168.1>
- Yanai, M., Esbensen, S., & Chu, J. (1973). Determination of bulk properties of tropical cloud clusters from large-scale heat and moisture budgets. *Journal of the Atmospheric Sciences*, *30*(4), 611–627. [https://doi.org/10.1175/1520-0469\(1973\)030<0611:DOBPOT>2.0.CO;2](https://doi.org/10.1175/1520-0469(1973)030<0611:DOBPOT>2.0.CO;2)